Kinetics of Noncatalytic, Nonisothermal, Gas-Solid Reactions: Hydrofluorination of Uranium Dioxide

EDUARDO C. COSTA and J. M. SMITH

University of California, Davis, California

A single-pellet, stirred-tank reactor was used to measure temperatures, compositions, and rates of reaction for the hydrofluorination of $UO_{2.14}$ at atmospheric pressure. By correlating the rate with conditions at the reacting surface, the activation energy of the first-order reaction was found to be 6,070 cal./g.-mole.

Since the product forms an unreactive layer around the core of $UO_{2.14}$, and since the heat of reaction is high, significant concentration and temperature differences develop between the gas phase and the reaction surface. The temperature and rate data were used to calculate the effective diffusivity and thermal conductivity of the product layer under reaction conditions.

An adaptation of a pseudosteady state method was developed for predicting the conversion and temperature history of a pellet. Using rate constants for reaction and mass and energy transfer derived from the experimental data, this method gave good results. Predictions with estimated rate constants were poor, indicating that an accurate value was necessary for the effective diffusivity in the product layer.

Reactions between gaseous and solid reactants to form solid and gaseous products provide a challenging combination of physical and chemical processes. If a solid reactant pellet is surrounded by the reactant gas, a layer of porous solid product of increasing thickness will form around the unreacted core. The overall reaction results from the following sequence of consecutive steps: mass transfer of reactant from the bulk gas to the outer surface of the pellet, diffusion through the porous product layer to the surface of the unreacted core, chemical reaction (combined with intrapellet diffusion if the solid reactant is porous), and, finally, diffusion of the product gas out through the layer of product and into the gas phase. There have been several isothermal analyses (*1* to *7*) of this type of process leading to prediction methods for the conversion of solid reactant as a function of time. However, if the heat of reaction and activation energy are appreciable, nonisothermal effects are important. Temperature differences between bulk gas and pellet surface will exist, and may be large even when concentration differences are negligible (*8*). Furthermore, intrapellet gradients will develop both in the product layer and unreacted core. Apparently the only treatment of the nonisothermal case is the analysis of Shen and Smith (*9*). They developed a conversion-time relationship for a spherical pellet of constant size undergoing a first-order reaction, in terms of the reaction and transport rate constants.

Very little well-defined experimental data are available for gas-solid noncatalytic reactions and none was found for the nonisothermal case. Cannon and Denbigh (*10*) presented a remarkable study of the oxidation of pellets of zinc oxide at different temperatures, and showed that a vapor phase could exist between the product layer and the unreacted core. However, they did not obtain conversion-time data.

It seemed to us that the proper test of a prediction method for the conversion-time relationship for nonisothermal conditions should consist of the following steps: (1) Determine experimentally the rate equation, including the activation energy, for the chemical step at the reacting interface. (2) Measure, or predict from available information, the rate constants for mass and energy transfer. (3) Obtain conversion-time data experimentally over a large interval. (4) Predict conversion and temperature versus time curves, using the rate constants from steps 1 and 2, for comparison with the data of step 3.

This procedure should be preferable to the simpler one of measuring only conversion-time data for comparison with the theory. The only evaluation in this second approach would be whether the rate constants, determined by fitting the conversion data, had reasonable values.

This paper is a report of the first approach applied to the hydrofluorination of porous spheres of nonstoichiometric (O/U = 2.14) uranium dioxide (UO_2) at nonisothermal conditions. This system was chosen in spite of the experimental difficulties in handling UO_2 and HF, because the kinetics of reacting pellets had not been studied heretofore using measured temperatures at the reacting interface. The experimental method was to suspend a pellet of $UO_{2.14}$ in a stirred-tank reactor and measure the pellet weight and temperatures as a function of time. Analysis of the data during the initial time period provided the information for step 1, while measurements for the whole time period up to high conversions provided the data for step 3. Intrapellet mass and energy rate constants for step 2 were evaluated from temperature and concentration measurements during a run. The work of Shen and Smith served as the basis for the prediction method used in step 4.

APPARATUS AND PROCEDURE

The apparatus (Figure 1) consisted of a hydrofluorination unit and a gas disposal section. The nitrogen and HF lines to the reactor were ¼-in. tubing of copper and Monel 400, respectively. Nitrogen flows were metered with glass rotameters and HF with a Kel-F rotameter. The disposal section received the gases from the reactor and consisted of a cooler (*11*), a spray-packed absorption column (*13*), and a water, suction pump (*14*). The latter maintained the reactor (*5*) at nearly atmospheric pressure and also dissolved any unabsorbed gases before disposal to the drain. An aqueous KOH solution was circulated through the absorber.

The stirred reactor (Figure 2) was built by joining two 2¼-in. I.D. hemispheres, press-formed out of 16 gauge Monel 400 plate.

Eduardo C. Costa is on leave from the Brazilian Atomic Energy Institute, Sao Paulo, Brazil.

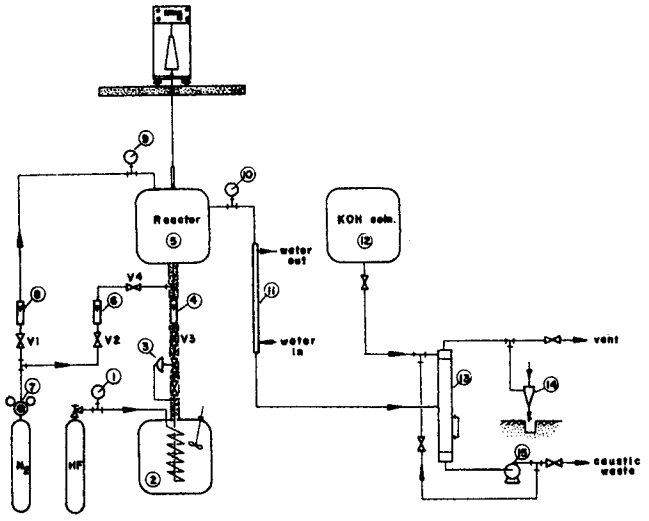

Fig. 1. Schematic diagram of the experimental apparatus. *1*, HF feed manometer. *2*, Constant temperature bath. *3*, HF flow regulator. *4*, HF feed rotameter. *5*, Reactor unit. *6*, Nitrogen feed rotameter. *7*, Nitrogen pressure regulator. *8*, Nitrogen chamber rotameter. *9*, Nitrogen chamber manometer. *10*, Reactor manometer. *11*, Cooler. *12*, Caustic supply tank. *13*, Absorption column. *14*, Water pump. *15*, Caustic circulation pump.

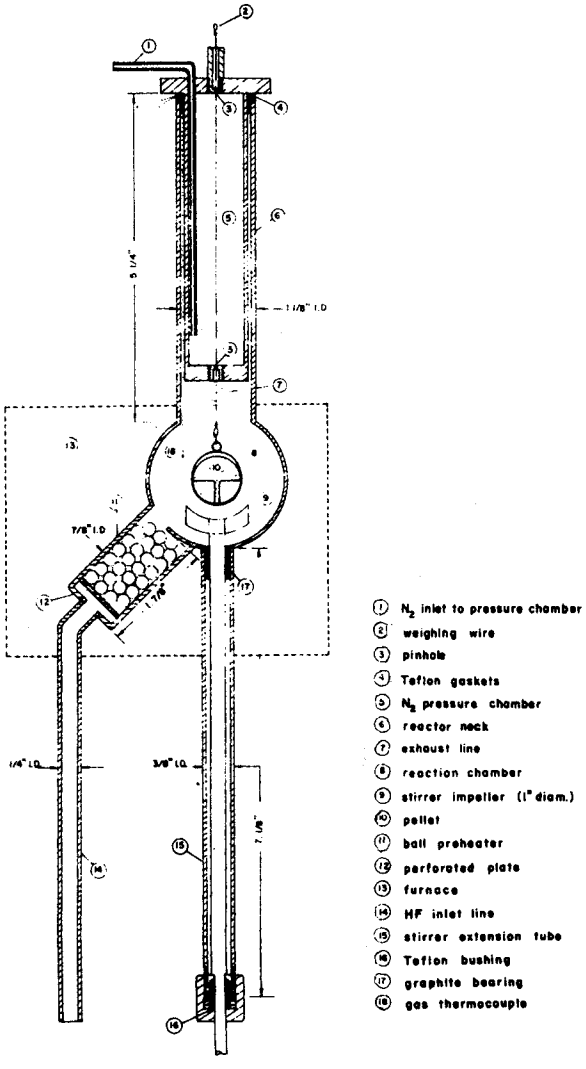

Fig. 2. Reactor detail.

A 1-in. diameter stirring blade was positioned in the reactor so that its upper edge was ¼-in. from the reacting pellet (see Figure 2). The stirrer speed could be varied from 200 to 1,720 r.p.m. The entire reactor was enclosed in a thermostatically controlled electric furnace. Also in the furnace was a preheater packed with ¼-in. Monel balls. The HF feed first passed through this preheater attaining a temperature determined by the furnace setting. Throughout the paper this is described as the HF feed temperature. It is equivalent to the temperature in the reactor at zero time, or the initial reaction temperature. This temperature level is used to identify a run. The gas, surface, and pellet-center temperatures within the reactor were higher than the HF feed temperature during reaction. The HF feed rate was 2.75 g.-moles/hr. for all runs.

The reaction was investigated from 30° to 367°C., a range which included the kinetic, unstable, and diffusion regimes. At each temperature level separate, identical runs were made for observing (1) the weight change and (2) the center and surface temperatures of the reacting pellet. In runs of the first type the gas temperature was also measured. In the second type the gas temperature was measured as well as temperatures at the center and surface of the pellet. Iron-constantan, 40-gauge thermocouples were used. The center temperature was measured by inserting a thermocouple in a $\frac{1}{64}$-in. hole drilled to the center of the pellet. The junction of the surface thermocouple was made about 2 cm. long by scraping and twisting together the iron and constantan wires. This junction was very slightly imbedded in a groove along the outer surface.

The pellet weight was measured to 0.1 mg. with a Mettler H-6, digital readout balance. The plate yoke underneath the balance was connected to a wire basket holding the pellet by a 0.02-in. soft-annealed Monel wire. The HF flow caused only a small (2 mg.) displacement from the weight at stagnant conditions. The fluctuation in the balance reading due to the stirrer was about 1 mg. at maximum speed.

A pressure chamber (see 5, Figure 2) containing nitrogen was used to prevent HF leakage through the $\frac{1}{32}$-in. hole for the wire holding the pellet. The nitrogen slowly flowed through the hole (3) and was removed through the outlet (7) by the suction of the water pump. This prevented HF leaving the reactor through the hole and also prevented air from the surroundings leaking into the reactor.

The pellets were slightly ellipsoidal with a long axis of 2.010 ± 0.020 cm. and a short axis of 1.97 ± 0.020 cm. (average radius = 0.996 cm.) They were prepared by compressing powder particles in a steel die, using camphor and stearic acid as binder and lubricant, respectively. These additives were subsequently eliminated by heating to 400°C. prior to sintering. The pellets were sintered, to impart mechanical strength, by heating for 2 hr. at 1,000°C. in a nitrogen atmosphere. Most of the data were obtained with pellets of 70% porosity, but a few initial rate measurements were also made with pellets of 63.6% porosity. The porosity was changed by adding different masses of $UO_{2.14}$ to the mold.

The uranium dioxide, from Nuclear Fuel Services, Inc., conformed to nuclear grade specifications. Anhydrous HF with a specified minimum purity of 99.9% was obtained from the Matheson Company.

PROPERTIES OF URANIUM DIOXIDE AND PRODUCT

Table 1 summarizes the properties of the $UO_{2.14}$ particles used to make the pellets. The physical properties of the unreacted, but sintered pellet and the layer of product UF_4 from each run are given in Table 2. The solid product is identified according to the HF feed temperature of the run. The true density of the solid was determined from the weight of the sample and its volume as measured with a Beckman air pycnometer. The total volume, needed to es-

TABLE 1. PROPERTIES OF URANIUM DIOXIDE PARTICLES

True density: 11.06 g./cu. cm.
O/U ratio: 2.14

Particle size distribution:

U.S. Standard Sieve No.	Microns	% Finer
60	250	87
100	149	75
140	105	38
200	74	14
325	44	2

TABLE 2. PROPERTIES OF THE SOLID REACTANT AND SOLID PRODUCT

HF feed temperature, °C.	True density ρ_t, g./cu. cm.	Apparent density ρ, g./cu. cm.	Porosities			Average pore diam. $2\bar{a}_a$, Å.	Macrosurface area, sq. m./g.
			Total ε_t	Macro ε_a	Micro ε_i		
Unreacted pellet	11.06	3.29	0.702	0.657	0.045	2740	2.91
69	9.48	3.43	0.640	0.594	0.046	2760	2.51
80	9.67	3.24	0.665	0.638	0.027	2820	2.80
85	9.26	3.14	0.662	0.610	0.052	2930	2.65
90	8.16	3.08	0.625	0.507	0.022	3000	2.21
100	8.53	3.02	0.645	0.635	0.010	2930	2.87
150	6.93	2.83	0.592	0.579	0.013	2530	3.24
250	6.68	2.76	0.586	0.565	0.021	2550	3.22
367	7.57	3.20	0.577	0.544	0.034	2400	2.83

tablish the apparent density of the porous solid, was determined by mercury displacement at atmospheric pressure. The total porosity was calculated from the densities by the expression

$$\varepsilon_t = 1 - \rho/\rho_t \tag{1}$$

Pore size distribution data were measured with a mercury porosimeter. This instrument had a maximum pressure such that equivalent cylindrical pores as small as 350 Å. can be penetrated. The macroporosity shown in Table 2 was the ratio of the volume of the pores ≥ 350 Å. to the total volume. The microporosity was determined by difference $\varepsilon_t - \varepsilon_a$ and is subject to uncertainty. In any event the difference is small, indicating that nearly all the pores are larger than 350Å. Thus the particles of $UO_{2.14}$ from which the pellet was made were essentially nonporous. The pores in the pellet and reaction product are due primarily to the space between original $UO_{2.14}$ particles.

The average macropore diameter was determined from the equation

$$\bar{a}_a = \frac{1}{V}\int_0^V a\,dV \tag{2}$$

The final column in Table 2 contains the macrosurface area, based upon cylindrical pores, and calculated by

$$S_a = \frac{4V}{\bar{a}_a}$$

Figure 3 gives the pore size distribution curves for the unreacted pellet and the porous product from the 150°, 250°, and 367°C. runs. Figure 3 and Table 2 show that the product has a slightly broader size range and a smaller porosity than the unreacted UO_2. Furthermore, the porosity of the product decreases with increasing reaction temperature, probably due to sintering and to plugging. Examination of the pellets after reaction at high temperatures indicated cracks in the product layer. The data in Table 2 and Figure 3 do not include the effects of cracks since the material was broken into small pieces (~⅛-in.) for the porosimeter measurements. The average pore diameters shown in Table 2 are large enough for bulk rather than Knudsen diffusion to govern mass transport.

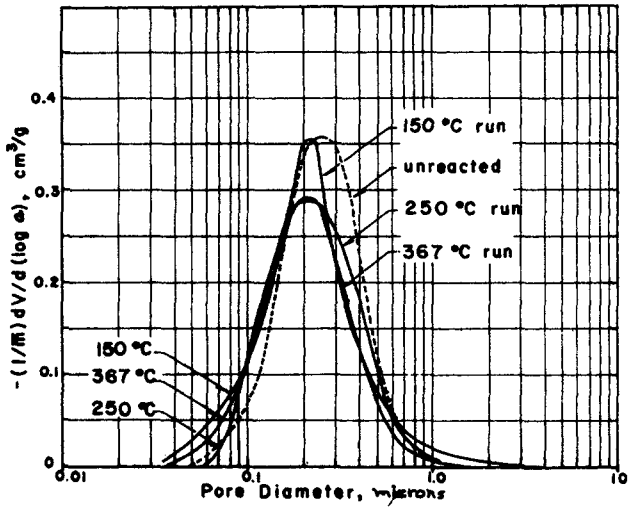

Fig. 3. Pore size distribution curves for the reactant (0.70 porosity) and reaction products of the 150°, 250°, and 367°C. runs.

HYDROFLUORINATION RESULTS

Calculation of the Rate

The $UO_{2.14}$ pellets behaved as mixtures of UO_2 and UO_3 (86% UO_2, 14% UO_3) which reacted to produce a product consisting of UF_4 and UO_2F_2, according to the reactions:

$$UO_2(s) + 4HF(g) \longrightarrow UF_4(s) + 2H_2O(g) \tag{3}$$

$$UO_3(s) + 2HF(g) \longrightarrow UO_2F_2(s) + H_2O(g) \tag{4}$$

A mass balance shows that the conversion X of $UO_{2.14}$ can be calculated from the measured pellet weight by the expression

$$X = 6.65\,(w/w_o - 1) \tag{5}$$

The rate of reaction was expressed as the moles of $UO_{2.14}$ reacting per unit surface at the radius r_c. This radius would locate the reaction interface, that is, the boundary between unreacted core of $UO_{2.14}$ and surrounding product layer, if the $UO_{2.14}$ were completely nonporous. A sharp reaction boundary of this type was observed at high temperatures (see later discussion). Even when the reaction occurred over a region, an equivalent value of r_c could be calculated from the total radius r_o by the expression

$$r_c = [r_o^3(1 - X)]^{1/3} \tag{6}$$

The apparent densities in Table 2 were used to calculate r_o. On this basis the rate was evaluated from the equation

$$-R = \frac{n_o}{4\pi r_c^2}\left(\frac{dX}{dt}\right) \tag{7}$$

using the experimental conversion-time data to establish the derivative. Water vapor concentrations in the reactor chamber, needed to evaluate the dependency of the rate upon concentrations, were calculated from the rate of reaction by assuming a well-mixed chamber and negligible holdup.

QUALITATIVE OBSERVATIONS

A plot of initial rates calculated from Equation (7) at $X \longrightarrow 0$ is shown in Figure 4. Three ranges of operation

are evident:

Initial reaction temp., °C.	Regime
30° to 90°	reaction control regime
90° to 200°	unstable region
200° to 367°	diffusion control regime

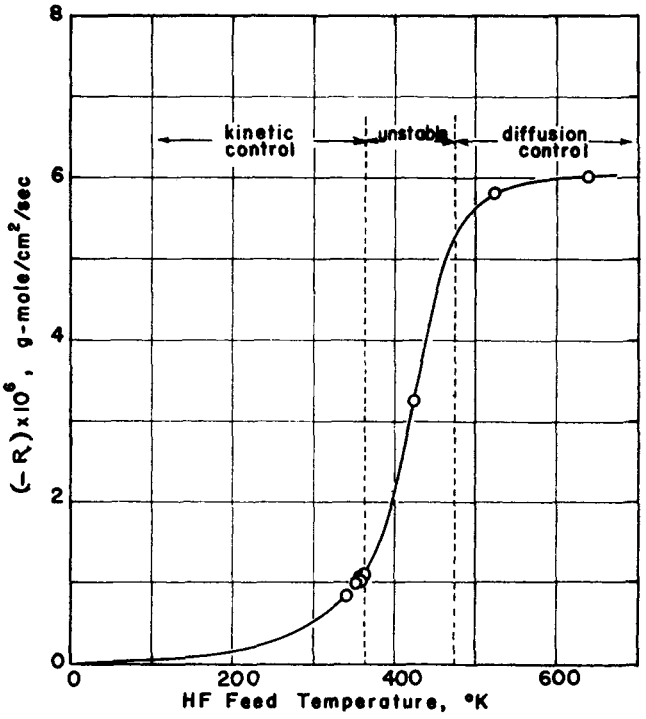

Fig. 4. Initial reaction rates versus HF feed temperatures.

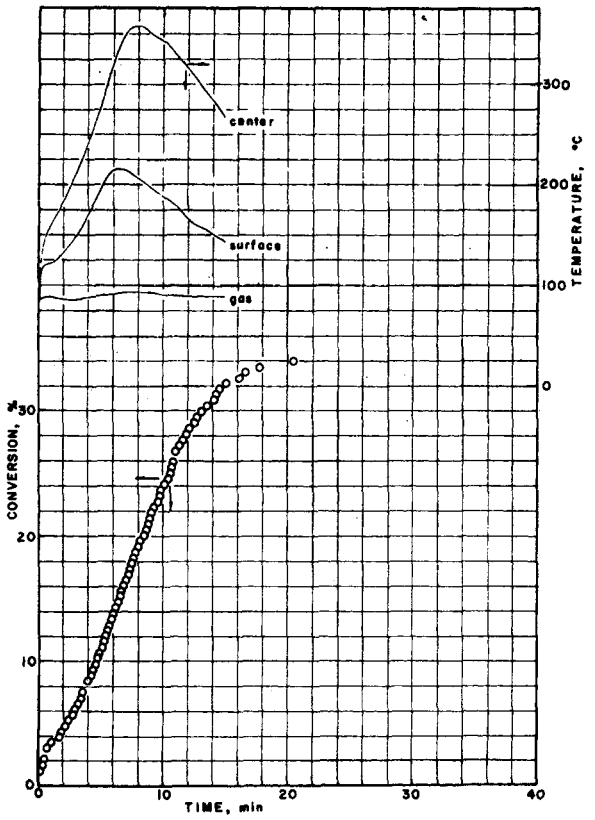

Fig. 5. Conversion versus time curve; run 30. Temperature versus time curve; run 34. HF feed temperature, 85°C; stirrer speed, 1,720 r.p.m.

In the kinetic region there was no visible boundary between reactant and product. Some increase in pellet size was observed after reaction, but no cracking occurred. The unreacted and reacted pellets were nearly indistinguishable. Figure 5 shows the conversion and temperature data for an 85°C. run. The temperatures were continuously recorded so that smooth curves are obtained. The circles on the conversion curve indicate times required to reach predetermined pellet weights. Since significant conversion occurred, it is concluded that reaction was relatively slow with respect to diffusion, even in the small void volume of the reactant. As a result reaction occurred across a large portion of the pellet diameter. At low temperatures HF is known to adsorb on UO_2 surfaces. The rapid increase in conversion in the initial section of the curve in Figure 5 is believed to be due to adsorption rather than reaction. This hump in the conversion versus time curve disappeared at high temperatures.

The initial rate increased rapidly with temperature above 90°C. For runs from 90° to 200°C. there was some distinction in appearance between reactant and product, although at 90°C. the reaction zone appeared to be as thick as 5 mm. This regime was characterized by rapidly changing temperatures, sharp local overheating at points inside the pellet, and the appearance of cracks in the later stages of the reaction.

At 250°C. there is no apparent local overheating; the final conversions are higher; and there is a sharper boundary between reactant and product. The cracks near the end of the reaction were larger. A diffusion-controlled reaction is indicated. Figure 6 shows that the maximum center

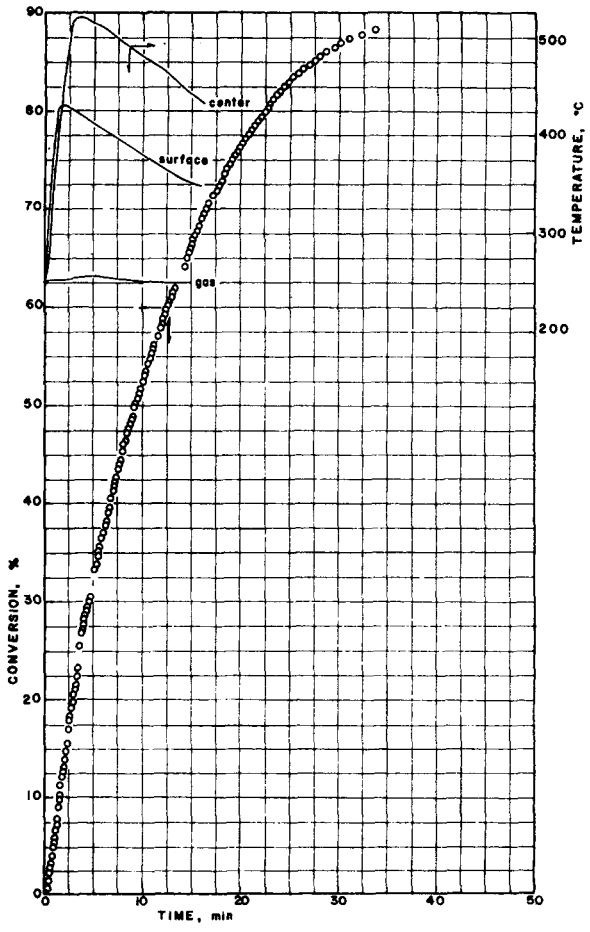

Fig. 6. Conversion versus time curve; run 8. Temperature versus time curve; run 11. HF feed temperature, 250°C.; stirrer speed, 1,720 r.p.m.

temperature of 520°C. is reached in 3.5 min. There was no evidence of sintering. The conversion curve appears to level off slightly below 100%. This is believed to be due to small granules of $UO_{2.14}$ becoming surrounded by relatively impermeable layers of product. At 357°C. there was a sharp definition between the light green of the product layer and the black-green color of the $UO_{2.14}$ core. No cracking was observed. Conversion stopped at 64%. Sintering of the product layer was believed to be the main cause for the absence of cracking and for the low final conversion.

Subsequent interpretation of the conversion-time data will be based upon a sharp interface, between reactant and material completely converted to product (that is, the so-called shrinking-core model is used). The qualitative discussion shows that this simple model is more realistic at higher temperatures. However, incomplete conversion even at long time periods at high temperatures, as shown in Figure 6, suggest an alternative explanation. Since the pellet was prepared from particles and has considerable porosity, perhaps conversion is limited because of an impermeable layer of product developing around individual particles within the pellet. In this view reaction would extend to the center of the pellet, but the conversion at any radial position would be incomplete. While visual observation does not provide an exact answer, the evidence indicates that this alternative explanation for incomplete conversion is more acceptable at low temperatures.

INTRINSIC RATE EQUATION

The experimental data permitted calculation of but one rate of reaction, according to Equations (5) and (7). Since the reactant pellets were 86% UO_2, the kinetic results will apply primarily to the hydrofluorination of UO_2 [Equation (3)]. Previous work (*11* to *13*) with UO_2 powder has shown the rate to be first order in HF. The mechanism is not well understood, but it has been postulated (*13*) that HF is first chemisorbed, and this is followed by a surface reaction. With this background the rate data were correlated by the equations

$$(-R) = k_r(c_{HF}) \tag{8}$$

$$k_r = k_o \exp(-E/RT) \tag{9}$$

The experimental values of c_{HF} and T can be used in these equations only when there are no diffusion resistances affecting the rate; that is, when there is a negligible product layer. Such conditions were satisfied during the initial period of a run. Hence k_o and E were evaluated from initial rate data using the surface thermocouple reading to obtain T_s. The importance of using the surface temperature rather than the gas temperature is evident from Figure 6, which shows that $T_s - T_g$ can be as much as 50° to 75°C. when the conversion is still but 1%.

The surface concentration of HF was calculated from the concentration in the gas phase and the mass transfer coefficient between gas and pellet surface. The gas in the reaction chamber contained only HF and H_2O. Hence

$$(x_{HF})_g = 1 - (x_{H_2O})_g \tag{10}$$

As mentioned $(x_{H_2O})_g$ was obtained from the rate of reaction by assuming complete mixing in the reactor. This assumption was tested by varying the stirrer speed. The mass transfer coefficient was predicted from the correlation

$$N_{Nu} = 2.0 + 0.6(N_{Re})^{1/2}(N_{Sc})^{1/3} \tag{11}$$

where $N_{Nu} = k_x(2r_o)/Dc_f$. The Reynolds number was based upon stirrer speed and pellet diameter:

$$N_{Re} = \frac{(2r_o)\,v_i\,\rho_g}{\mu} \tag{12}$$

The experimental temperature data provided some justification for use of Equations (11) and (12). $T_s - T_g$ was first calculated from the energy balance

$$4\pi r_s^2 h(T_s - T_g) = 4\pi r_s^2(-R)(-\Delta H) \tag{13}$$

using a heat transfer coefficient obtained from Equation (11) with $N_{Nu} = h(2r_o)/k$ and with the Prandtl number replacing N_{Sc}. The calculated and experimental temperature differences were then compared. Typical results are given in Table 3. The agreement is reasonable except for the 250° and 367°C. runs. At these high temperatures the rate of heat transfer into the core of unreacted pellet is about as large as the rate out into the gas phase. Hence Equation (13), which neglects this term, is not valid. The concentration differences $(x_g - x_s)_{HF}$ calculated using Equation (11) for k_x are shown in the next to the last column of Table 3. Note that these values are small, so that the importance of using the surface concentration is not as critical as using the surface temperature in Equations (8) and (9).

The values of $k_{r,s}$ calculated from Equation (8) are shown in Figure 7 for the pellets of both porosities. The deviations from the Arrhenius equation at low temperatures probably have two causes: physical adsorption which accompanies reaction gives an apparent rate that is too high; and the reaction occurs over a region of the pellet with an effective area larger than the outer surface, again giving an apparent rate per unit surface that is too high. At higher temperatures the plot is linear and corresponds to

$$k_r = 46 \exp(-6070/R_gT) \tag{14}$$

Equation (14) will be used to evaluate the intrinsic rate in the conversion and temperature predictions. The absence

TABLE 3. TEMPERATURE AND CONCENTRATION DIFFERENCES BETWEEN PELLET AND GAS

HF feed temperature, °C.	Stirrer speed, r.p.m.	Time, min.	$(T_s - T_g)_{exp}$, °C.	$(T_s - T_g)^*_{calc.}$, °C.	$(x_g - x_s)^\dagger_{HF}$
80	1,720	2.5	34	51	0.013
85	1,720	2.2	49	53	0.014
90	1,720	1.9	62	57	0.015
150	1,720	1.25	146	153	0.044
250	1,720	1.5	181	253	0.077
367	1,720	1.25	95	265	0.079
85	550	3.5	137	157	0.040
85	550	5.0	202	259	0.070

*Calculated from Equation (13) using heat transfer coefficients from Equation (11) with N_{Pr} substituted for N_{Sc}.

†Calculated using mass transfer coefficients from Equation (11).

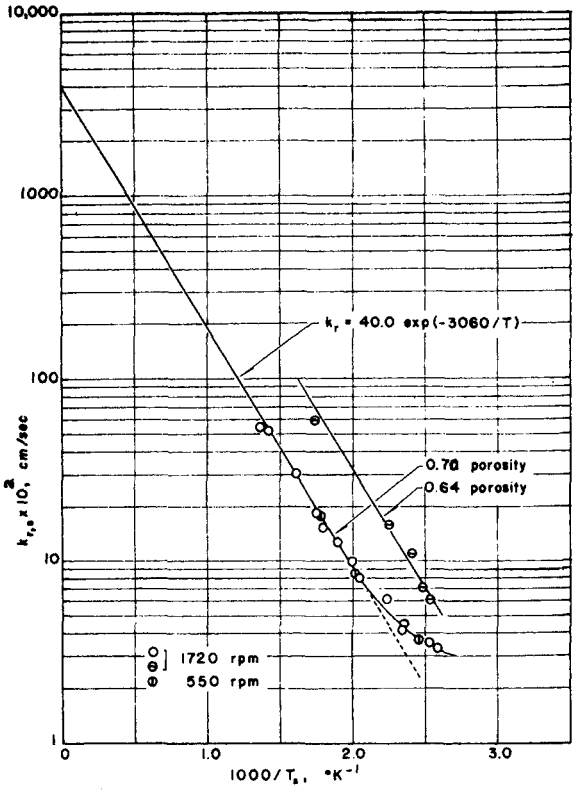

Fig. 7. Arrhenius plot for initial rate data.

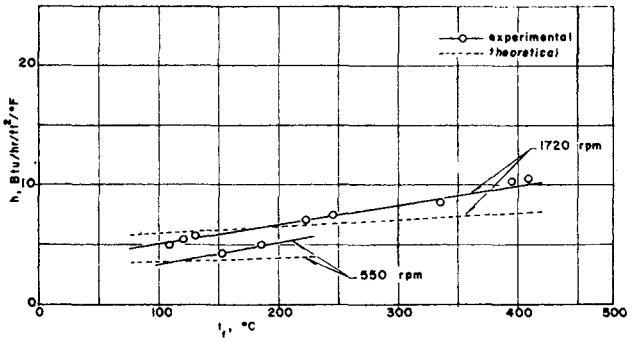

Fig. 8. Heat transfer coefficients.

of effect of stirrer speed lends confidence to the assumption of complete mixing in the gas.

The activation energy of 6.07 kcal./mole agrees reasonably well with 6.93 reported for the hydrofluorination of pure UO_2 by Ellis and Roberts (*12*). Their measurements were on a polished surface of UO_2 under conditions where temperature differences between gas and solid surface were probably negligible. Other literature data range from 7.1 to 10.1 kcal./mole, but many of these results were obtained where the reaction temperature could have been significantly different from the measured value. The rate for the pellet of lower porosity is about three times higher, although the activation energy is unchanged. This difference is much greater than expected from the area increase associated with the porosity change. The degree of compression of the $UO_{2.14}$ particles in initially forming the pellet appears to affect the reactivity of the solid surface. Perhaps the sintering process changes the surface to an extent dependent upon the initial porosity.

MASS AND ENERGY TRANSPORT

Gas-to-pellet and intrapellet (product layer) heat and mass transfer rates are needed for predicting conversion-time behavior. These rate constants were evaluated, for the main part, from the experimental measurements, as described in the following paragraphs.

Pellet-to-Gas Coefficients

Heat transfer coefficients, assumed to be constant around the pellet, were calculated from Equation (13) using observed temperature and rate of reaction data. This expression is a valid energy balance when there is no heat flow into the unreacted core; that is, when the center temperature is approximately constant with time. Reference to Figures 5, 16, and 14 indicates that this will be true only at times when the center thermocouple reading is at or slightly beyond the maximum value, where the center cools slowly. The points in Figure 8 show the results of the calculations for both stirrer speeds. Also included as dotted lines are the lines calculated from Equations (11) and (12). The heat of reaction used, −42 kcal./g.-mole, is a combination of ΔH for reactions (2) and (3) according to the composition of the pellet (86% UO_2, 14% UO_3).

Since the experimental and calculated heat transfer coefficients agreed well, Equations (11) and (12) were also used to evaluate mass transfer coefficients between pellet and gas.

Intrapellet Transport Properties

The shell model, which supposes a sharp boundary between product and unreacted core, will be used to predict the conversion and temperature history of a pellet. Also a pseudosteady state with respect to the reaction interface is assumed. That is, the velocity of mass or energy through the product layer is assumed to be rapid with respect to the velocity of the reaction interface. The same assumptions are made here to calculate thermal conductivity and diffusivity of the product layer under reaction conditions. The thermal conductivity k_{ef} was obtained from an energy balance at the reaction interface, neglecting energy exchange with the unreacted core. Hence only the data after the temperature maximum could be used. The temperature at the reaction interface was not measured. However, in the time region where the core cools slowly, the interface temperature will be nearly equal to the center temperature. With these assumptions, the energy balance at the reaction interface is

$$R(\Delta H) = -k_{ef}\left(\frac{dT}{dr}\right)_{r_c} \tag{15}$$

The pseudosteady state condition permits a simple calculation of the temperature profile through the product layer. Use of this profile to evaluate the gradient at r_c gives

$$-\left(\frac{dT}{dr}\right)_{r_c} = \frac{1}{r_c^2}(T_c - T_s)\Big/\left(\frac{1}{r_c} - \frac{1}{r_s}\right) \tag{16}$$

The total radius of the pellet changed somewhat with extent of reaction but could be calculated from the apparent densities of product and $UO_{2.14}$ by the expression

$$r_s^3 = r_c^3 + \frac{(M/\rho)_p}{(M/\rho)_{UO_{2.14}}}(r_o^3 - r_c^3) \tag{17}$$

Using Equations (15) to (17), k_{ef} was calculated for temperatures from 150° to 367°C. The results, shown in Figure 9, exhibit a sharper temperature effect than expected. The points designated by the same feed gas temperature were evaluated at different times during the same run. The 150°C. run results are much lower than the others. Such factors as cracking and sintering, and the severe assumptions made in the evaluation, probably account for the

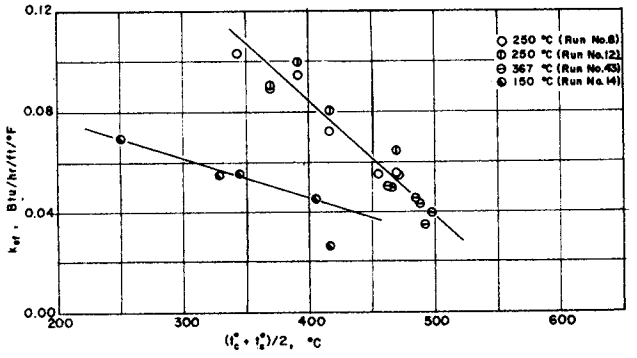

Fig. 9. Experimental effective thermal conductivities.

steep temperature dependency. In the qualitative observations the differences between the 150°C. and higher temperature runs were noted. The magnitude of the data in Figure 9 is similar to that for porous catalysts (*14*) measured under nonreacting conditions.

Effective diffusivities for HF-H_2O in the pores of the product layer were evaluated by the same procedure as used for k_{ef}. The mass balance at the reaction interface is

$$4(-R) = N_{HF} = -D_{ef}\,c\left(\frac{dx_{HF}}{dr}\right) + x_{HF}\,(N_{HF} + N_{H_2O})$$

Since $N_{H_2O} = -\frac{1}{2}N_{HF}$ this may be written as

$$4(-R) = -\left(\frac{D_{ef}\,c}{1 - x_{HF}/2}\right)\frac{dx_{HF}}{dr} \qquad (18)$$

The gradient in Equation (18) is calculated by differentiating the concentration profile. The pseudosteady state condition permits the profile to be obtained by integrating Equation (18) through the product layer, with $-4R$ taken as constant. This integration is not difficult, but the logarithmic term obtained introduces considerable complexity when the profile is used in the prediction method. Therefore it is of interest to see if a simpler profile, derived by integrating the equimolal counter diffusion simplification of Equation (18), would give nearly the same diffusivities. Using this simpler approach and assuming that the temperature varies linearly with radius and that the diffusivity is constant, the gradient evaluated at r_c is

$$\frac{dx_{HF}}{dt} = \left(\frac{m}{r_c} - \frac{b}{r^2}\right)\frac{(x_s - x_c)_{HF}}{m\ln\left(\frac{r_s}{r_c}\right) - b\left(\frac{1}{r_c} - \frac{1}{r_s}\right)} \qquad (19)$$

where

$$m = \frac{T_c - T_s}{r_s - r_c} \qquad (20)$$

$$b = (r_s\,T_c - r_c\,T_s)/(r_s - r_c) \qquad (21)$$

The gradient given by Equation (19) was used in Equation (18) to calculate D_{ef}. The values of $(x_{HF})_c$ were obtained from $-R$ and T_c using Equations (8) and (9) evaluated at r_c, and with k_o and E given by Equation (14). The results are shown in the last column of Table 4 and in Figure 10. If equimolal diffusion is not assumed, an expression more complicated than Equation (19) results for the gradient, but D_{ef} can still be determined. These values are given in the next to last column of Table 4. The two sets agree within ±10%. Hence the simpler approach will be used.

In the absence of experimental diffusion or reaction data, porosities may be used with the random pore model (*15*) to estimate D_{ef}. Neglecting diffusion in the small volume of micro pores, and assuming that bulk diffusion controls the process in the porous product, one finds the prediction equation to be

$$(D_{ef})_{calc} = \varepsilon_a^2 D \qquad (22)$$

These results, given in Table 4, are much larger than the experimental values for the 367°C. run, although the agree-

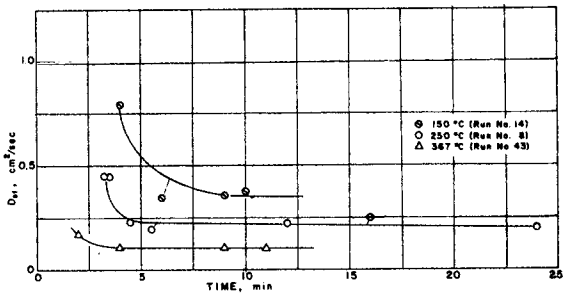

Fig. 10. Experimental effective diffusivities.

Table 4. Effective Diffusivities in Product Layer

HF feed temperature, °C.	Time, min.	Temperature range,* °K.	D,† sq. cm./sec.	Calc. D_{ef},‡ sq. cm./sec.	D_{ef},§ sq. cm./sec.	D_{ef},‖ sq. cm./sec.
367	2	771 ± 38	1.56	0.44	0.17	0.16
	4	762 ± 38	1.52	0.43	0.11	0.095
	9	739 ± 42	1.43	0.40	0.11	0.092
	11	735 ± 39	1.42	0.40	0.10	0.080
250	3.25	740 ± 44	1.44	0.45	0.45	0.43
	3.5	743 ± 49	1.45	0.46	0.45	0.42
	4.5	739 ± 50	1.43	0.45	0.23	0.20
	5.5	733 ± 51	1.41	0.45	0.19	0.16
	12	690 ± 51	1.27	0.40	0.22	0.22
	16	665 ± 44	1.18	0.37	0.25	0.21
	24	617 ± 35	1.03	0.33	0.19	0.16
150	4	690 ± 74	1.27	0.43	0.79	0.74
	6	679 ± 81	1.23	0.41	0.35	0.31
	9	618 ± 76	1.03	0.35	0.36	0.34
	10	602 ± 78	0.98	0.33	0.38	0.35

*Average of the center and surface temperatures..
†Molecular diffusivity calculated from the Chapman-Enskog relationship.
‡Calculated from random pore model [Equation (22)].
§From experimental data using $N_{HF} = -2N_{H_2O}$.
‖From experimental data assuming equal molal counter diffusion [Equations (18), (19)].

ment at lower temperatures is about all that could be expected. It is possible that sintering blocks off a significant fraction of the pores at high temperatures, thus reducing the diffusivity. The effect of temperature level is also apparent in Figure 10. The rapid fall in D_{ef} with time is probably due to plugging of pores, due to expansion while the product is formed. The effects of sintering, which increases with temperature, perhaps explain the relative position of three curves. Note that the temperature of the product layer changes with time along any one curve in Figure 10. However, temperatures for the 367°C. run were always higher than those for the 250°C. run. These results suggest that diffusivities are very sensitive to effects of cracking, sintering, and plugging of the pores. This makes accurate prediction of D_{ef} a difficult task.

PREDICTION OF CONVERSION AND TEMPERATURE CURVES

With the intrinsic rate equation established and values available for the transport rate constants, the tools are at hand for predicting temperature and conversion as a function of time. The method used is that of a uniformly shrinking, unreacted core with an expanding product layer. Pseudosteady state is assumed for mass transfer (*16*). The same assumption is less suitable for calculating the temperature profile in the product layer, because there can be significant heat transfer from the reaction interface at r_c into the core. Hence Equation (15) is not valid and also the center temperature will change rapidly with time. Comparison of Figures 5, 6, and 15 indicates that the effect will be more severe at high temperatures. Shen and Smith (*9*) developed a prediction method neglecting heat exchange with the core. This method will be compared first with the data, and then an unsteady state modification will be introduced to correct for the inadequacy of Equation (15).

Pseudosteady State

The geometry of the model is shown in Figure 11. The temperature throughout the unreacted core is assumed to be uniform and equal to the value at r_c. Also the temperature in the gas phase is taken as uniform and equal to the initial reaction temperature, despite the heat of reaction. That is, the small variation in gas temperature with time shown in Figures 5 and 6 is neglected. The method involves the simultaneous solution of the following mass and energy transfer equations:

Pellet-to-Gas

$$\text{mass transfer: } -\left(\frac{1}{4}\pi r_s^2\right)\frac{dn_{HF}}{dt} = 2k_x(x_g - x_s)_{HF} \tag{23}$$

$$\text{heat transfer: } Q = 4\pi r_s^2 h(T_s - T_g) \tag{24}$$

Product layer

$$\text{mass transfer: } -\left(\frac{1}{4}\pi r^2\right)\frac{dn_{HF}}{dt} = \left[\frac{cD_{ef}}{1 - x_{HF/2}}\right]\frac{dx_{HF}}{dr} \tag{25}$$

$$\text{heat transfer: } Q = 4\pi r^2 k_{ef}\left(-\frac{dT}{dr}\right) \tag{26}$$

Reaction Surface

$$\text{mass transfer: } -\left(\frac{1}{4}\pi r_c^2\right)\frac{dn_{HF}}{dt} = 4(-R) \tag{27}$$

$$\text{heat transfer: } Q = 4\pi r_c^2 R(\Delta H) \tag{28}$$

The solution method employed is analogous to that given by Shen and Smith (*9*). Major differences are (1) r_s is not assumed to be constant, but is calculated from r_c by Equation (17), and (2), a somewhat different solution procedure

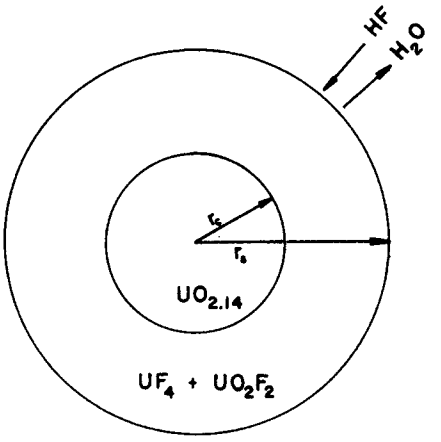

Fig. 11. Geometry of reacting pellet.

was found more suitable for rapid machine computation. A set of four simultaneous equations derived from Equations (23) to (28) was solved for T_c, T_s, $(x_{HF})_c$, and $(x_{HF})_s$ in terms of r_c. Then the time to attain various r_c values was calculated by integrating the expression

$$t = \frac{\rho}{(M)_{UO_{2.14}}}\int_{r_c}^{r_o}\frac{dr_c}{(-R)} \tag{29}$$

R was evaluated from T_c and (x_{HF_c}) using Equation (9) applied at $r = r_c$. Finally, the conversion could be calculated from Equation (6).

Predicted results were obtained for the 150°C. case as well as for 250 and 367°C. Heat and mass transfer coefficients employed were those given in Figures 8 and calculated from Equations (11) and (12) at a stirrer speed of 1,720 r.p.m. Constant average values were used throughout a run. Similarly, single values of k_{ef} and D_{ef} were used and evaluated from Figures 9 and 10 by averaging all the values for the pertinent run. Only the nearly flat portion of the curves for D_{ef} were used in the averaging process. In Table 5 are summarized the values of all the parameters employed in the calculations.

TABLE 5. DATA FOR THE CONVERSION AND TEMPERATURE PREDICTIONS

Parameter	150°C. Run	250°C. Run	367°C. Run
Initial reaction temperature T_g, °K.	423	523	640
HF feed flow rate, g.-moles/sec.	7.6×10^{-4}	7.6×10^{-4}	7.6×10^{-4}
Initial pellet weight w_o, g.	12.903	12.970	12.861
Apparent density of the product ρ, g./cu. cm.	2.83	2.76	3.07
Heat of reaction $(-\Delta H)$, kcal./mole	42	42	42
Frequency factor k_o, cm./sec.	40	40	40
Activation energy E, kcal./mole	6.07	6.07	6.07
Mass transfer coefficient k_x, g.-mole/(sq. cm.)(sec.)	1.5×10^{-4}	1.52×10^{-4}	1.53×10^{-4}
Heat transfer coefficient h, cal./(sq. cm.)(sec.)(°C.)	9.7×10^{-4}	11.6×10^{-4}	13.9×10^{-4}
Effective thermal conductivity k_{ef}, cal./(cm.)(sec.)(°C.)	2.08×10^{-4}	2.76×10^{-4}	1.87×10^{-4}
Effective diffusivity D_{ef}, sq. cm./sec.	0.36	0.22	0.11
Reynolds number	880	605	550

The conversions and temperatures predicted by this method are compared with the experimental data for the 150° and 367°C. runs in Figures 12 to 15. The conversion results are in good agreement until higher values are reached. As mentioned earlier the deviation for the 150°C. run may be due to trapping of unreacted granules of $UO_{2.14}$ which are surrounded by a product layer; at this temperature the reaction takes place over a region of the unreacted core. It is surprising how well the conversions agree, since the unreacted core model is not realistic at this temperature (see qualitative observations). Deviations in the temperature curves are large, particularly for the center point. At 367°C. the agreement between predicted and experimental conversions is better in the range 0 to 60%, presumably because the unreacted core model is a better representation than at 150°C. At high conversions the experimental value falls below the predicted curve, because of sintering of the product layer at the high temperatures involved. Particularly at 367°C. the calculated temperatures peak too early and reach too high levels. The agreement at 250°C., between predicted and experimental conversions, was somewhat better than at 150° and 367°C. but the temperature comparisons were similar to those in Figure 15.

Unsteady State

The unreacted core temperature is again assumed to be uniform and equal to the value at r_c. However, Equation (28) is replaced by

$$\frac{d}{dt}\left[(nC_p)_{UO_{2.14}}(T_c - T_o)\right] = 4\pi r_c^2 R(\Delta H) - 4\pi r_c^2 k_{ef}\left(-\frac{dT}{dr}\right)_{r_c} \quad (30)$$

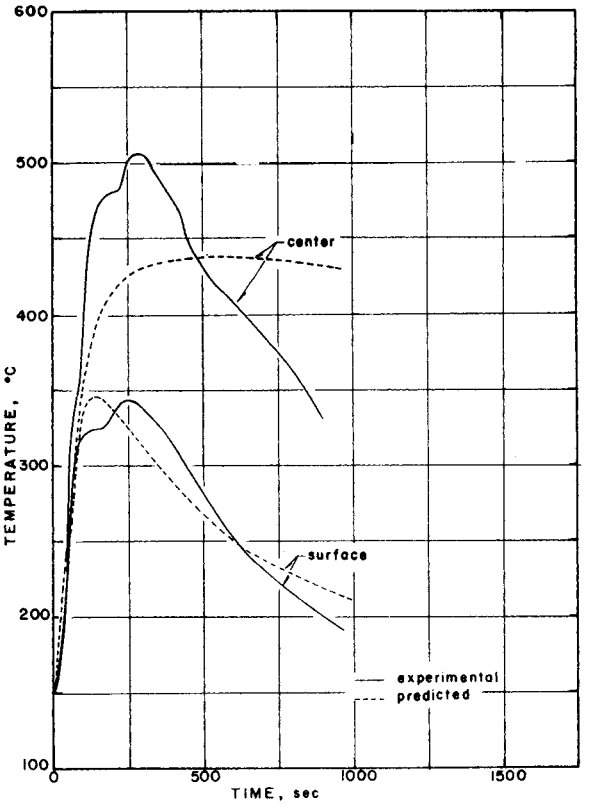

Fig. 13. Experimental and predicted temperature curves. HF feed temperature, 150°C.; stirrer speed, 1,720 r.p.m.; initial pellet weight, 12.903 g.

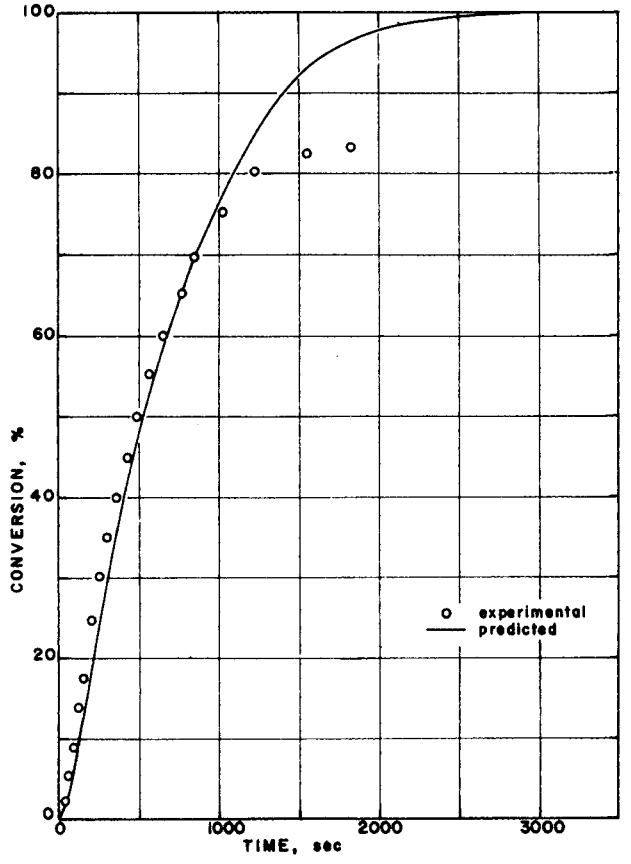

Fig. 12. Experimental and predicted conversion curves. HF feed temperature, 150°C.; stirrer speed, 1,720 r.p.m.; initial pellet weight, 12.903 g.

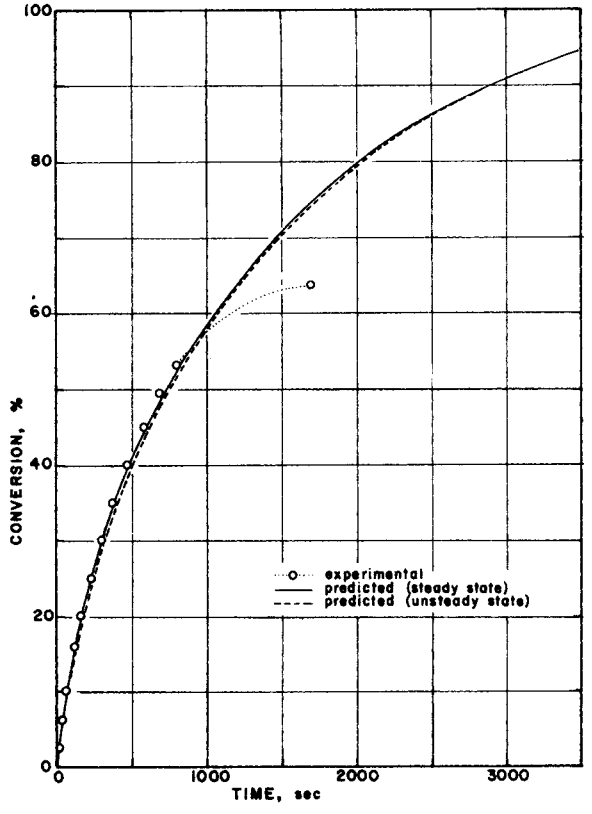

Fig. 14. Experimental and predicted conversion curves. HF feed temperature, 367°C.; stirrer speed, 1,720 r.p.m.; initial pellet weight, 12.861 g.

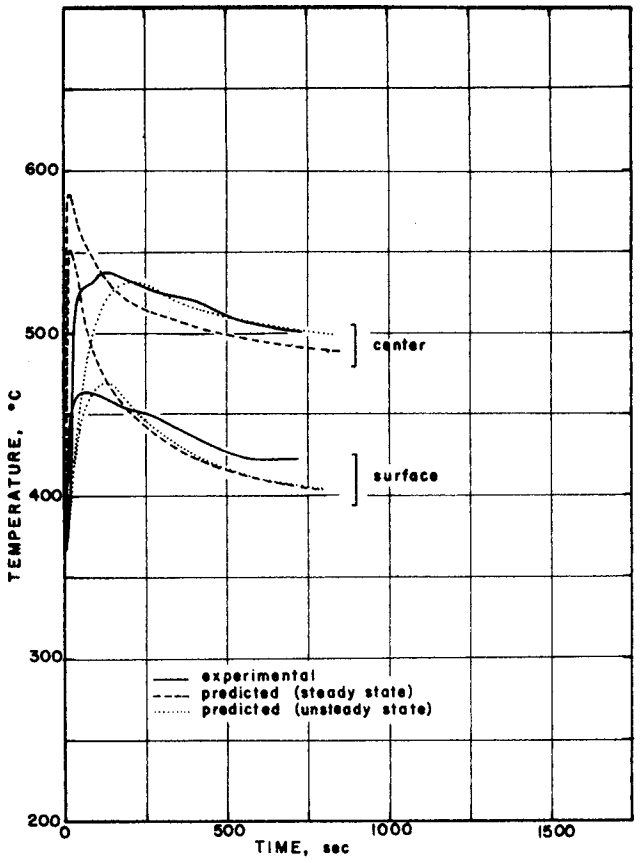

Fig. 15. Experimental and predicted temperature curves. HF feed temperature, 367°C.; stirrer speed, 1,720 r.p.m.; initial pellet weight, 12.861 g.

Also the moles of unreacted $UO_{2.14}$ are related to R and r_c by

$$\frac{dn_{UO_{2.14}}}{dt} = -4\pi r_c^2 (-R) \tag{31}$$

$$n_{UO_{2.14}} = \frac{4}{3}\pi r_c^3 \rho / M_{UO_{2.14}} \tag{32}$$

These three equations now replace Equation (28) for the heat transfer part of the problem. Note that Q given by Equations (24) and (26) is the same, even though it is not equal to the heat of reaction. Hence, evaluating Equation (26) at $r = r_s$ and equating Q from it to Equation (24) gives another relationship for T_s. The problem is now completely defined and the mass and energy transfer equations can be solved simultaneously for T_s, T_c, $(x_{HF})_c$, and $(x_{HF})_g$ at various values of r_c. The rest of the calculations are the same as for the pseudosteady state method.

The results are shown for the 367°C. run in Figures 14 and 15 by the indicated lines. In comparing the two methods the conversion curve is nearly unchanged but in the unsteady state method the temperature peak is reduced and shifted to longer times, in better agreement with the experimental results. In fact the maximum in the curves for both center and surface temperatures agrees very well with the data. However, the time required to reach the peak has increased beyond the experimental result.

Results with Estimated Transport Properties

The ultimate goal in treating gas-solid noncatalytic reactions would be to predict conversion curves from rate constants estimated from correlations or available data. It is not possible even to approximate the intrinsic rate equation, but data and methods exist for estimating thermal conductivities and diffusivities of porous solids. Table 6 compares the estimated transport constants with those obtained for the 367°C. run. Pellet-to-gas rate constants were obtained from existing correlations, for example, Equation (11). The effective diffusivity was estimated from the random pore model (*16*) using a porosity of 0.70, the value for the unreacted core. This would be the only a priori value. Comparison of the D_{ef} values shows that this was a poor assumption, since this high porosity was partially responsible for D_{ef} being five times greater than the result from Table 5. The effective thermal conductivity was estimated from data on UF_4 (*17*), and is in reasonably good agreement with the experimental value. In fact all the other rate constants in Table 6 are approximately the same as used in the previous predictions (Table 5, 367°C.). Figures 16 and 17 compare the predicted and experimental

Table 6. Estimated Transport Rate Constants

Property	367°C. Run	
	Predicted	Experimental
Macropore void fraction, ε_a^*	0.70	0.53
Apparent density of the product, g./cu. cm.	2.01	3.07
Effective diffusivity, sq. cm./sec.	0.54	0.11
Effective thermal conductivity, cal./(cm.)(sec.)(°C.)	1.6×10^{-4}	1.87×10^{-4}
Heat transfer coefficient, cal./(sq. cm.)(sec.)(°C.)	10×10^{-4}	13.9×10^{-4}
Mass transfer coefficient, g.-mole/(sq. cm.)(sec.)	1.52×10^{-4}	1.53×10^{-4}

*Predicted from Equations (11) and (12).

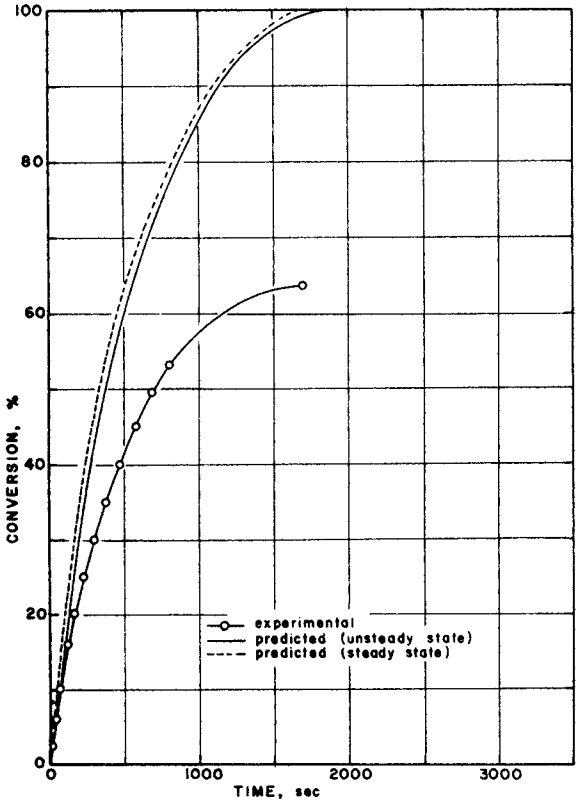

Fig. 16. Experimental and predicted conversion curves from estimated rate constants. HF feed temperature, 367°C.; stirrer speed, 1,720 r.p.m.; initial pellet weight, 12,861 g.

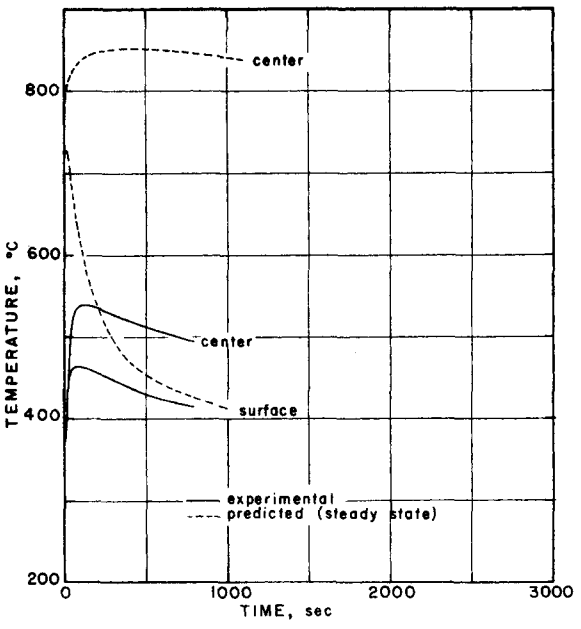

Fig. 17. Experimental and predicted temperature curves from estimated rate constants. HF feed temperature, 367°C.; stirrer speed, 1,720 r.p.m.; initial pellet weight, 12.861 g.

data. The agreement is poor for both conversion and temperatures. Evidently an accurate value of D_{ef} is important if reliable predictions are to be made. This requires first that the porosity of the product layer be known accurately. If the correct porosity of 0.53 had been known, the diffusivity predicted by the random pore model Equation (22) would have been reduced from 0.54 to 0.31 sq. cm./sec. This is still much larger than the experimental value of 0.11, so that the random pore model itself is not suitable in this application. The model does not take into account the changing structure during reaction, as caused by plugging of the pores and sintering of the solid product.

CONCLUSIONS

The results show that temperatures and concentrations at the reaction surface must be used to correlate intrinsic reaction rates. It is demonstrated that such properties can be measured continuously by using a large single pellet in a stirred-tank reactor. From these data effective thermal conductivities and diffusivities of the product layer can be evaluated under reaction conditions.

By combining the intrinsic rate equation with appropriate mass and energy transport limitations, conversion versus time curves could be predicted which agreed well with experimental results. Temperature predictions were not satisfactory using a pseudosteady state method because of heat transfer into the unreacted core of the pellet, particularly at high temperatures. However, a simple unsteady state method corrected much of the error in the predicted temperature.

Reliable estimates of mass and energy transfer coefficients between pellet and gas could be made from available correlations. This was not possible for the effective diffusivity in the product layer, presumably because existing methods do not account for the effects of cracking, plugging of the pores, and sintering. Also predicted temperatures and conversions are both sensitive to the value used for the diffusivity.

Two conclusions specific to the hydrofluorination reaction are of interest. First, at low temperatures physical adsorption of HF, superimposed upon the reaction, gives erroneously high, apparent rates of reaction. Second, a change in pellet porosity causes a shift in the frequency factor of the Arrhenius equation, but does not change the activation energy.

ACKNOWLEDGMENT

The authors thank the Brazilian Nuclear Energy Commission and the Atomic Energy Institute of Sao Paulo, Brazil, for fellowship support. Also the financial assistance of the National Science Foundation, Grant No. 2990, is acknowledged.

NOTATION

a = pore diameter, μ or Å; $\bar{a}$ denotes average value
c = gas concentration, g.-mole/cu. cm.
C_p = molar heat capacity at constant pressure, cal./(g.-mole)(°C.)
D_{ef} = effective diffusivity, sq. cm./sec.
D = molecular diffusivity of HF–H_2O system, sq. cm./sec.
E = activation energy of reaction, cal./g.-mole
h = heat transfer coefficient between pellet and gas, cal./(sq. cm.)(sec.)(°C.)
ΔH = heat of reaction, cal./g.-mole of solid reactant
k = thermal conductivity, cal./(cm.)(sec.)(°C.)
k_{ef} = effective thermal conductivity of the product layer, cal./(cm.)(sec.)(°C.)
k_o = frequency factor in the Arrhenius equation, cm./sec.
k_r = reaction rate constant, cm./sec.
k_x = mass transfer coefficient, g.-mole/(sq. cm.)(sec.)
M = molecular weight, g./g.-mole
$\bar{m}$ = mass of porosimeter sample, g.
n = moles of any substance
n_o = initial moles of $UO_{2.14}$ in a pellet
N = mass flux in the radial direction in the product layers, g.-mole/(sq. cm.)(sec.)
N_{Nu} = Nusselt number for heat transfer = $2r_o h/k$
= Nusselt number for mass transfer = $2r_o k_x/Dc_f$
N_{Pr} = Prandtl number
N_{Re} = Reynolds number
N_{Sc} = Schmidt number
O/U = atomic ratio of oxygen to uranium
p = pressure, atm.
Q = rate of heat flow, cal./sec.
r = radial position in the pellet, cm.
$-R_{HF}$ = rate of formation of HF, g.-mole/(sq. cm.)(sec.)
$-R$ = rate of formation of $UO_{2.14}$, g.-mole/(sq. cm.)(sec.)
R_g = universal gas constant
S = macrosurface area, sq. m./g.
t = time, sec.
T = absolute temperature, °K.
T_g = HF feed temperature or initial reaction temperature, °K.
v_i = velocity of the stirrer, cm./sec.
V = volume of mercury compressed into the sample (porosimeter experiments), cu. cm./g.
x = mole fraction in the gas phase
X = fractional conversion of $UO_{2.14}$
w = weight of the reacting pellet at any time, g.
w_o = initial weight of the pellet, g.

Greek Letters

ε_a = macropore void fraction
ε_i = value of ε_t minus the value of ε_a
ε_t = total pore void fraction
ρ = apparent density of the porous solid, g./cu. cm.
ρ_t = true density of the solid in the pellet, g./cu. cm.
μ = gas viscosity, g./(cm.)(sec.)

Subscripts

avg = average
c = evaluated at the radius of the unreacted core, that is, at the reaction surface

f = evaluated at the average film temperature, $t_f^\circ = (t_s^\circ + t_g^\circ)/2$
g = evaluated at conditions of the gas in the reaction chamber
o = evaluated at the initial conditions
p = solid product
r = solid reactant
s = evaluated at the external surface of the pellet

LITERATURE CITED

1. Beveridge, G. S. G., and K. G. Denbigh, *Trans. Inst. Chem. Eng.*, **40**, 23 (1962).
2. Dunoyer, J. M., *J. Chim. Phys.*, **47**, 290 (1950).
3. Jost, W., *Chem. Eng. Sci.*, **2**, 199 (1953).
4. Levenspiel, O., "Chemical Reaction Engineering," Chap. 12, Wiley, New York (1962).
5. Philbrook, W. O., F. S. Manning, and M. A. Osman, *AIChE J.*, **12**, 685 (1966).
6. Weisz, P. B., and R. D. Goodwin, *J. Catalysis*, **2**, 397 (1963).
7. Tamman, G., *Z. Anorg. Chem.*, **111**, 78 (1920).
8. Maymo, J. A., and J. M. Smith, *AIChE J.*, **12**, 845 (1966).
9. Shen, J., and J. M. Smith, *Ind. Eng. Chem. Fundamentals*, **4**, 293 (1965).
10. Cannon, K. J., and K. G. Denbigh, *Chem. Eng. Sci.*, **6**, 145 (1957).
11. DeMarco, R. E., D. C. Bonfer, and R. C. Abbot, *USAEC Rept. NLCO-675 (Apr. 1957)*.
12. Ellis, W. P., *J. Chem. Phys.*, **39**, 1172 (1963).
13. Tomlinson, L., S. A. Morrow, and S. Graves, *Trans. Faraday Soc.*, **57**, 1008 (1961).
14. Satterfield, C. N., and T. K. Sherwood, "The Role of Diffusion in Catalysis," p. 87, Addison-Wesley, Reading, Mass. (1963).
15. Wakao, Noriaki, and J. M. Smith, *Chem. Eng. Sci.*, **17**, 825 (1962).
16. Bischoff, K. B., *ibid.*, **18**, 711 (1963).
17. Belle, J., ed., "Uranium Dioxide: Properties and Nuclear Applications," U.S. Atomic Energy Commission, U.S. Govt. Printing Office, Washington D. C. (1961).

Manuscript received April 21, 1969; revision received October 2, 1969; paper accepted October 6, 1969.

Experimental Heats of Mixing for Gaseous Nitrogen and Methane

R. R. KLEIN, C. O. BENNETT, and B. F. DODGE

Yale University, New Haven, Connecticut

The excess enthalpy of binary gas phase mixtures has been measured by direct experiment, using a continuous flow, isothermal calorimeter. Heat of mixing data are presented for the methane-nitrogen system for compositions of 25 to 80 mole % methane in nitrogen, at temperatures of 40°, 0°, −20°, −40°, −60°, and −78°C. and pressures from 250 to 1,500 lb./sq. in. abs. These data are in agreement with the literature to within the experimental uncertainty of this work, 4%.

The experimental results agree well with values predicted using the Benedict-Webb-Rubin and the Redlich-Kwong equations of state. The virial equation of state truncated after the third coefficient fits the low density data only. The liquid theories of Scott predict the enthalpies of the mixtures in a qualitative way.

The heat of mixing or excess enthalpy is defined by the equation

$$H^E = H_m - \sum_i y_i H_i \quad \text{(constant } p \text{ and } T\text{)} \qquad (1)$$

It provides one means of obtaining the enthalpy of solutions whose practical importance for the design and analysis of heat exchange equipment is obvious. It is also of scientific importance since it provides a test of mixing rules for an equation of state and a test of theories of molecular interactions. Experimental data on the enthalpy of gas mixtures are quite limited and engineers have been obliged to calculate values needed for design by various approximate methods.

R. R. Klein is at Uniroyal Corporation, Naugatuck, Connecticut. C. O. Bennett is at the University of Connecticut, Storrs, Connecticut.

METHODS OF PREDICTING H_m

Before describing the experiments it seems appropriate to consider various ways by which H_m can be calculated. The differential equations relating H_m to the variables of state are well known and rigorous but their integration requires either an equation of state or the equivalent pressure-volume-temperature data. The application of equations of state to a mixture involves empirical mixing rules whose validity is uncertain, and in many cases there are no experimental data against which to test the methods. In the course of this work we have tested three equations of state: a modified Redlich-Kwong (R-K) equation, the Benedict-